



Evolution of SiO₂ matrix during the formation of Ge and Si nanocrystals by ion implantation

U. Serincan *, S. Yerci, M. Kulakci, R. Turan

Department of Physics, Middle East Technical University, 06531 Ankara, Turkey

Received 25 February 2005; received in revised form 27 April 2005
Available online 5 July 2005

Abstract

Fourier transformed infrared spectroscopy (FTIR) has been employed to observe and understand structural variations in SiO₂ matrix during the formation of Ge and Si nanocrystals by ion implantation as a function of processing parameters. The Si–O asymmetric stretching peak of absorption spectra were used to monitor the evolution of SiO_x ($x < 2$) films during the annealing process. It was shown that the recovery process in Si–O network is quite different in Ge and Si implanted samples and the deformation caused by Ge atoms in the SiO₂ matrix can be recovered by annealing the implanted samples at lower temperatures than that by Si atoms. This is in agreement with the formation kinetics of the Si and Ge nanocrystals in SiO₂ as observed by Raman spectroscopy and photoluminescence measurements of the same samples.

© 2005 Elsevier B.V. All rights reserved.

PACS: 78.30.L; 61.46

Keywords: Si; Ge; Nanocrystal; SiO₂; FTIR

1. Introduction

Luminescence and charge storage properties of semiconductor nanocrystals embedded in dielectrics like SiO₂ are expected to lead to the development of new photonic and microelectronic devices.

Size dependent light emission from these nanostructures and their charge storage capabilities have been demonstrated for different material and matrix structures in recent years [1–16]. The major consequences of these phenomena will be the fabrication of light emitting devices tunable with the nanocrystal size; and fabrication of more reliable, denser and more robust flash memory cells [1,3,11–13]. These developments are likely to have revolutionary impacts in the Si based

* Corresponding author. Tel.: +90 312 210 3280; fax: +90 312 210 1281.

E-mail address: serincan@metu.edu.tr (U. Serincan).

microelectronic and photonic technology in the near future.

Due to the compatibility with the existing Si technology, group IV elements, mostly Ge and Si, have been subject of investigation for the nanocrystal formation in SiO₂ and other matrices [1–8]. As shown by many research groups including the authors of this paper, Ge and Si nanocrystals with well-defined spherical shape can be formed in the dielectric matrices by ion implantation followed by a high-temperature annealing process [2,17–19]. Some of the expected optical and electrical behaviors of these nanocrystals are already demonstrated [1,11,16]. The major challenge reported by these groups is however to overcome the problems in the production of well-controlled, uniform and reproducible nanostructures with the desired electrical and optical properties. This requires an extensive and comparative study of the production techniques, matrix or substrate materials, processing and chemical structure of nanocrystals and the matrix with new approaches.

Measurement of nanocrystals in a matrix is a challenging issue due to the difficulties in probing embedded structures with nanometric size. Although it is possible to observe Si nanocrystals in SiO₂ matrix by high-resolution transmission electron microscopy (HR-TEM) [20], having the same structure with the substrate and presence of Si in the matrix material, Si nanocrystals in SiO₂ matrix grown on a Si substrate are hardly distinguishable with common techniques such as Raman spectroscopy and standard transmission electron microscopy with relatively low resolution. Most of the recently published reports on Si nanocrystals embedded in SiO₂ are therefore based on the photoluminescence measurements with limited structural evidence [21–23]. It is quite desirable to improve the metrology of the nanostructures with new experimental approaches. In this paper we report on the FTIR analysis of the nanocrystal/dielectrics system in order to monitor the structural evolution of the matrix material rather than the nanocrystals themselves. Such an analysis would provide not only evaluation of the matrix for potential device applications but also an indirect method for the diagnosis of the nanocrystals. A comparative study of SiO₂ matrix containing Ge

and Si nanocrystals is presented in this work. The recovery of the matrix during the annealing process is monitored by FTIR and the comparison of Ge and Si nanocrystal formation are shown to provide information on both the nanocrystal formation and structural variation of the matrix material. As a supplementary evidence, Raman spectroscopy and photoluminescence results are also discussed.

2. Experiment

Thermally grown 250 nm thick SiO₂ films on (100)Si wafers were implanted with ⁷⁴Ge or ²⁸Si ions at an energy of 100 keV with fluences between 1×10^{16} and 1.5×10^{17} cm⁻². The projected range (R_p) of the Ge and Si ions were calculated by using the TRIM software [24] as 70.0 and 140.0 nm, respectively. Samples were annealed at 800–1250 °C for 1 or 2 h under N₂ atmosphere. Presence of Ge nanocrystals was verified by Raman spectroscopy measurements. PL experiments were conducted at room temperature with an excitation source of 532 nm NdYAG laser. Emitted light was detected with a MS-257 type monochromator and a Hamamatsu CCD camera. FTIR spectroscopy was used in the absorbance mode (350–2500 cm⁻¹, 2 cm⁻¹ resolution) to monitor the Si–O asymmetric stretching peak, its intensity and full-width at half-maximum (FWHM). Samples were measured under the same experimental conditions for comparison.

3. Results and discussion

3.1. Observation of nanocrystal formation

We reported previously extensive studies on the formation of Ge nanocrystals in the SiO₂ matrix [18,19]. It was there shown that formation of Ge nanocrystal takes place by a segregation/precipitation process at annealing temperatures as low as 700 °C. Formation of Ge nanocrystals in the samples studied in this work has been verified by Raman spectroscopy measurements as a function of annealing temperature (not shown here). From

the finger print Raman signal appeared at 300 cm^{-1} , it was concluded that all samples studied contain Ge nanocrystals after the annealing process and their density increases with the annealing temperature. This is consistent with our previously reported results including extensive Raman analysis of Ge nanocrystals [25].

Formation of Si nanocrystals has been verified by using PL spectroscopy. It is well-established that light emission from Si implanted SiO_2 falls generally into two region of the light spectrum: an emission at the wavelength of about 600 nm which is usually attributed to the defects and structures other than nanocrystals, and an emission at about 700–850 nm which results from the nanocrystals [22,26]. PL spectra of Si implanted and annealed samples at $900\text{ }^\circ\text{C}$ and $1050\text{ }^\circ\text{C}$ for 2 h are shown in Fig. 1. It is observed from this figure that the sample annealed at $1050\text{ }^\circ\text{C}$ exhibits a strong PL band at $\sim 850\text{ nm}$ while the sample annealed at $900\text{ }^\circ\text{C}$ exhibits a weak emission at $\sim 650\text{ nm}$. Although there is still a debate on the exact mechanism of the light emission, one can certainly conclude that PL band seen at $\sim 850\text{ nm}$ is related to the presence of Si nanocrystals in the matrix [27]. For detailed descriptions of Raman and PL spectra of Ge and Si implanted SiO_2 films see [25,27], respectively.

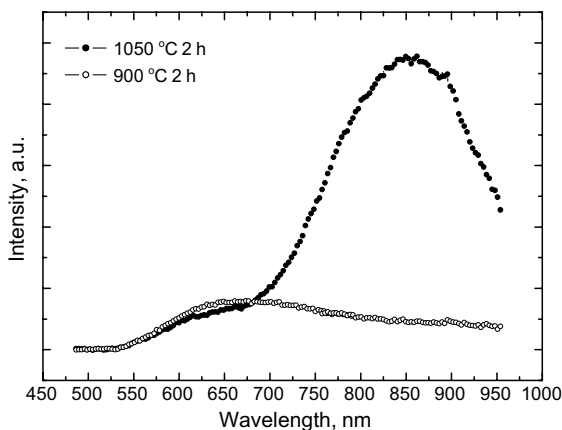


Fig. 1. PL spectra of a sample which is implanted with Si at a fluence of $1.5 \times 10^{17}\text{ cm}^{-2}$ at 100 keV and annealed at $900\text{ }^\circ\text{C}$ and $1050\text{ }^\circ\text{C}$ for 2 h under N_2 atmosphere.

3.2. FTIR study of the SiO_2 matrix

FTIR spectra of Si implanted samples as a function of annealing temperature and a non-implanted oxide are shown in Fig. 2. The major features observed from the absorption spectra of the implanted samples are a redshift, broadening and decrease in intensity of the Si–O–Si bond stretching vibration peak (at $\sim 1075\text{ cm}^{-1}$). In addition to these, two shoulders are observed at the high- and low-frequency side of the main silica stretch mode. The high-frequency shoulder of the main silica stretch mode is due to the contribution of the LO Si–O vibration mode [28]. The effect of ion implantation manifests itself as the formation of non-stoichiometric oxide with $x < 2$. This is understandable because of two main effects of Si ion implantation into SiO_2 . The introduction of excess Si into the matrix and the breaking Si–O bonds during slowing down of the implanted atoms. Upon annealing at sufficiently high temperature the deformed oxide bonds start to recover as excess Si atoms precipitate to form nanoparticles, leading to decrease in the shoulder seen in the lower wave number side of the FTIR curve. Therefore, the low-frequency shoulder can be related to the presence of excess Si in the SiO_2 matrix and the

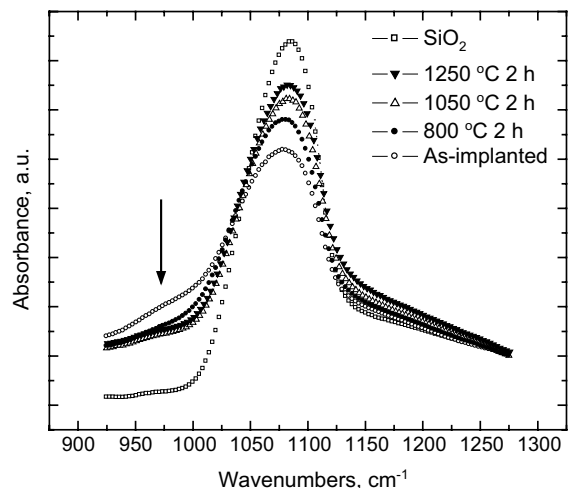


Fig. 2. FTIR spectra of a Si implanted sample at a fluence of $1.5 \times 10^{17}\text{ cm}^{-2}$ at 100 keV. Shoulder formation is indicated by an arrow.

substoichiometric oxide matrix formed during ion implantation.

Fig. 3 depicts FTIR spectra obtained from Ge implanted samples. We see that the as-implanted sample exhibits a similar feature to that of Si implanted sample. The same shoulder resulted from the deformation in the SiO₂ matrix is seen in the lower wave number side of the main peak. However, there are significant differences between the FTIR spectra of the Ge and Si implanted samples. A comparison of Figs. 2 and 3 reveals that the recovery of Si–O networks occurs at much lower temperatures in the case of the Ge implantation. This situation can be explained as follows: excess Ge and Si ions in the SiO₂ matrix deformed the Si–O bond structure by bonding with O or Si. For example in the case of Ge implantation, Si–O bonds were broken and some Si–Ge–O, Ge–Ge, Ge–O, Si–Si and Si–Ge and individual dangling bonds are formed [29]. During the annealing process, the excess Ge and Si atoms leave their initial positions and form clusters of a few nanometers. This segregation process is observed in the absorption spectra as the reduction of the shoulder (recovery of the stoichiometry of the SiO₂ matrix) as shown in Figs. 2 and 3. It is well-known that Ge atoms are not soluble in SiO₂ and completely segregated out of the growing oxide if one oxidizes Si crystal containing Ge atoms [30]. This is due to the

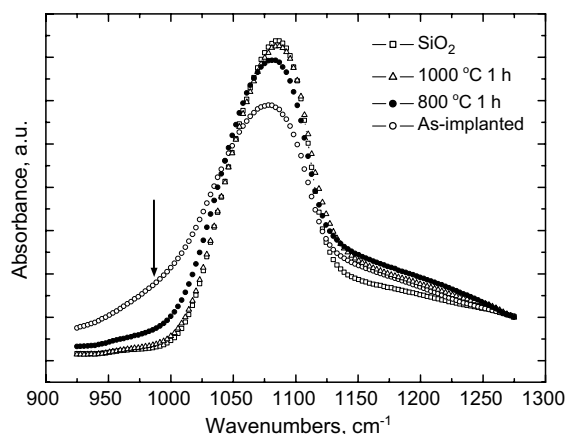


Fig. 3. FTIR spectra of a Ge implanted sample at a fluence of $1.5 \times 10^{17} \text{ cm}^{-2}$ at 100 keV. Shoulder formation is indicated by an arrow.

fact that the formation of SiO₂ is thermodynamically more favorable than the formation of GeO [31] and that the binding energy of the Si–O bonds (8.3 eV) is greater than that of Ge–O (6.8 eV). In addition to the precipitation in the matrix, we showed that some Ge atoms are segregated on the underlying Si substrate [19]. The rejection of Ge by the SiO₂ matrix leads to high diffusivity for Ge atoms, resulting in the formation of Ge nanoparticles at temperatures lower than for Si nanoparticles.

This situation can also be perceived from Fig. 4, where FWHM of the spectra is plotted against the annealing temperature. The FWHM of the Si–O stretching peak is a measure of the chemical and structural perfectness of the film. We see from the FWHM of the Ge implanted sample that the recovery process starts at relatively low temperatures and approaches that of pure SiO₂ film (i.e. 70 cm^{-1}) with a higher rate than the Si implanted sample. On the other hand, the FWHM of the Si implanted sample is significantly higher than that of pure SiO₂ after annealing at 1250 °C, indicating that the segregation and recovery process of the Si from the SiO₂ matrix is not completed even after annealing at such a high temperature.

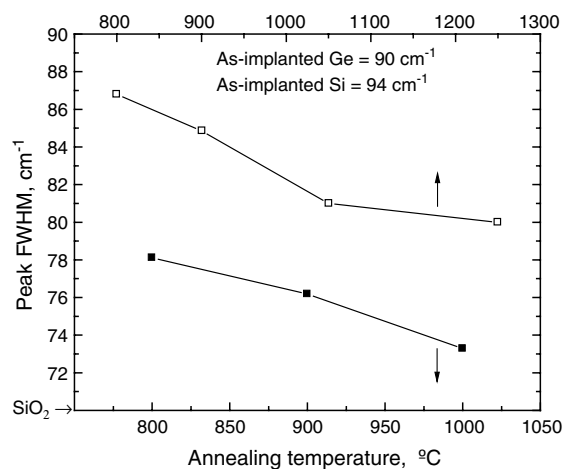


Fig. 4. Annealing temperature dependence of FWHM of the Si–O stretching peak, obtained from Ge- (closed squares) and Si-implanted (open squares) samples. For reference, the non-implanted SiO₂ and corresponding as-implanted values are also indicated. Annealing times for the Ge- and Si-implanted samples are 1 and 2 h, respectively. Lines are guides to the eyes.

The intensity and the position of the absorption peak provide additional information on the structural changes in the matrix. The variations in the intensity of the absorption peaks normalized to the pure SiO_2 are shown in Fig. 5. The difference in the variation of peak intensity for Si and Ge implanted samples as a function of annealing temperature shows the same correlation with the Si and Ge nanocluster formation in the SiO_2 matrix. In the case of Ge implanted sample, the signal intensity increases significantly at 800 °C and reaches almost the same value as that of the sample annealed at 1000 °C. This indicates again that Ge segregation from the SiO_2 matrix is almost completed at very low temperatures. For the Si implanted sample, the variation in the peak intensity is small at 800 °C compared to that of as-implanted and is significant for 1250 °C annealing. However, at that temperature the peak intensity is still lower than that of pure SiO_2 , indicating again that segregation of Si from the oxide matrix is not completed even after annealing at this temperature.

The frequency shift in the absorption spectra indicates a structural change in the material. As can be identified from Figs. 2 and 3, the position

of the absorption peak of the as implanted samples shifts slightly towards the lower wave numbers (i.e. redshift). This redshift could be interpreted as the narrowing of the O–Si–O bond angle due to the replacement of O atoms by the implanted atoms [32]. It is observed that this redshift is around 6.0 and 6.2 cm^{-1} from 1085.4 cm^{-1} for thermally grown SiO_2 for Ge and Si as-implanted samples, respectively. Upon annealing between 800 and 1250 °C, the shift is reduced down to 0.1 cm^{-1} for Ge and 2.4 cm^{-1} for Si implanted samples as a result of Ge and Si segregation/precipitation. The peak frequency of the Ge implanted sample approaches that of virgin SiO_2 film quicker than the Si implanted sample, showing again that SiO_2 recovers itself faster in the case of Ge implantation as a result of Ge segregation at lower temperatures compared to that of Si.

The variation of the matrix deformation and subsequent the recovery of the SiO_2 layer with the fluence of Si implantation is shown in Fig. 6. The normalized absorption intensity Si–O stretching peak increases with decreasing implantation fluence for the samples annealed at 1050 °C for 2 h as expected. It is seen that the sample implanted with 10^{16} cm^{-2} Si is almost fully recovered

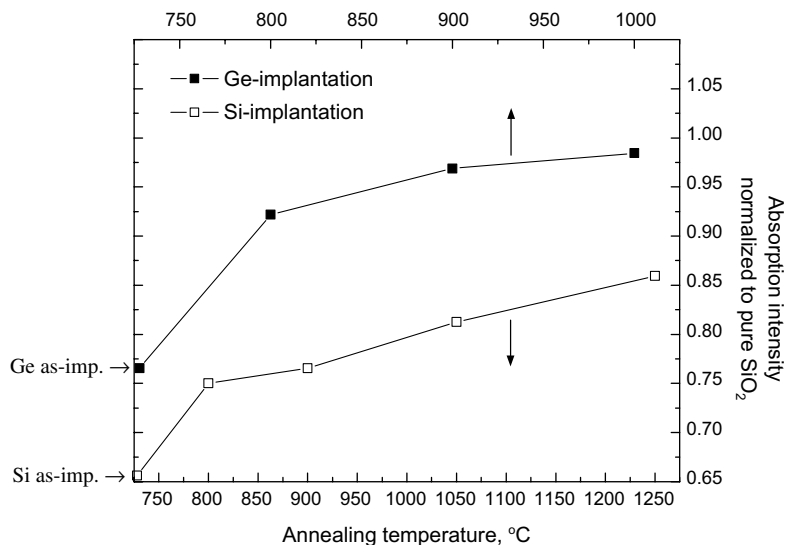


Fig. 5. Annealing temperature dependence of absorption intensity of the Si–O stretching peak, obtained from Ge- and Si-implanted samples. For reference, the as-implanted values are also indicated. Annealing times for the Ge- and Si-implanted samples are 1 and 2 h, respectively. Lines are guides to the eyes.

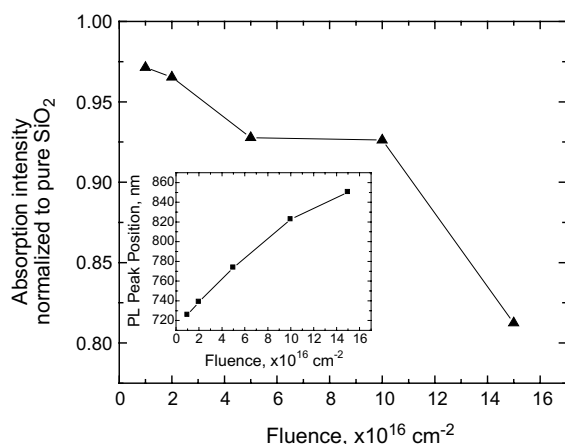


Fig. 6. Fluence dependence of absorption intensity of the Si–O stretching peak, obtained from samples implanted with Si and annealed at 1050 °C for 2 h under N₂ ambient. PL peak position as a function of implantation fluence for the same samples is designated in the inset. Lines are guides to the eyes.

after the annealing while the samples with higher fluences remain partially recovered. Based on the above results, the recovery is expected to improve with an annealing at higher temperatures and durations. It is however important to note that PL emission data indicates the formation of the nanocrystals in all these samples even with very short annealing duration at the annealing temperature of 1050 °C. The presence of the nanocrystals in the matrix is evidenced by the size dependence of the PL emission. The peak position of the PL emission red shifted as the implantation fluence increases. This data is displayed in the inset of Fig. 6 for the sake of completeness.

4. Conclusion

FTIR spectroscopy was employed to study the Ge and Si implanted samples to observe and understand Ge and Si nanocrystal formation in SiO₂ matrix as a function of processing parameters. The correlation between structural variations in the SiO₂ matrix and nanocrystal formation was studied by monitoring the recovery of Si–O networks. We have made a comparison between 1.5×10^{17} cm⁻² Ge and Si implanted samples and

found that the structural deformation caused by Ge atoms in the SiO₂ matrix can be recovered by annealing the implanted samples at 800 °C for 1 h under N₂ ambient while for the Si implanted samples the recovery process could not be completed after annealing at 1250 °C for 2 h. This is in agreement with our Raman and PL measurements and with other reported results of formation kinetics of Ge and Si nanocrystal formation. It is also important to note that in the case of Si ion implantation, for implantation fluences higher than 10^{16} cm⁻², although Si nanocrystals are formed after annealing the implanted samples at 1050 °C for 2 h the segregation of Si from the SiO₂ matrix and thus the formation process is not completed.

Acknowledgement

This work has been supported by the European FP6 project SEMINANO with the Contract No. 505285.

References

- [1] P. Normand, E. Kapetanakis, P. Dimitrakis, D. Skarlatos, K. Beltsios, D. Tsoukalas, C. Bonafos, G. Ben Assayag, N. Cherkashin, A. Claverie, J.A. Van Den Berg, V. Soncini, A. Agarwal, M. Ameen, M. Perego, M. Fanciulli, Nucl. Instr. and Meth. B 216 (2004) 228.
- [2] B. Garrido, M. López, A. Pérez-Rodríguez, C. García, P. Pellegrino, R. Ferré, J.A. Moreno, J.R. Morante, C. Bonafos, M. Carrada, A. Claverie, J. de la Torre, A. Souifi, Nucl. Instr. and Meth. B 216 (2004) 213.
- [3] M. Kanoun, M. Lemiti, G. Bremond, A. Souifi, F. Bassani, I. Berbezier, Superlattices Microstruct. 36 (2004) 143.
- [4] S. Kim, S.-H. Choi, C.J. Park, H.Y. Cho, R.G. Elliman, J. Korean Phys. Soc. 45 (2004) 501.
- [5] J. de La Torre, A. Souifi, A. Poncet, C. Buseret, M. Lemiti, G. Bremond, G. Guillot, O. Gonzalez, B. Garrido, J.R. Morante, C. Bonafos, Physica E 16 (2003) 326.
- [6] G.-R. Lin, J. Appl. Phys. 94 (2003) 7542.
- [7] Z. Pei, H.L. Hwang, Appl. Surf. Sci. 212 (2003) 760.
- [8] W. Skorupa, L. Rebohle, T. Gebel, Appl. Phys. A 76 (2003) 1049.
- [9] E. Borsella, C. de Julián Fernández, M.A. García, G. Mattei, C. Maurizio, P. Mazzoldi, S. Padovani, C. Sada, G. Battaglin, E. Cattaruzza, F. Gonella, A. Quaranta, F. D'Acapito, M.A. Tagliente, L. Tapfer, Nucl. Instr. and Meth. B 191 (2002) 447.

- [10] G. Franzò, A. Irrera, E.C. Moreira, M. Miritello, F. Iacona, D. Sanfilippo, G. Di Stefano, P.G. Fallica, F. Priolo, *Appl. Phys. A* 74 (2002) 1.
- [11] T. Matsuda, M. Kawabe, H. Iwata, T. Ohzone, *IEICE Trans. Electron.* 85 (2002) 1895.
- [12] J. von Borany, T. Gebel, K.-H. Stegemann, H.-J. Thees, M. Wittmaack, *Solid State Electron.* 46 (2002) 1729.
- [13] H.-J. Thees, M. Wittmaack, K.-H. Stegemann, J.v. Borany, K.-H. Heinig, T. Gebel, *Microelectron. Reliab.* 40 (2000) 867.
- [14] C.W. White, A. Meldrum, J.D. Budai, S.P. Withrow, E. Sonder, R.A. Zuhr, D.M. Hembree Jr., M. Wu, D.O. Henderson, *Nucl. Instr. and Meth. B* 148 (1999) 991.
- [15] I.E. Tyschenko, V.A. Volodin, L. Rebohle, M. Voelskov, V. Skorupa, *Semiconductors* 33 (1999) 523.
- [16] C.L. Heng, Y.J. Liuc, A.T.S. Wee, T.G. Finstad, *J. Cryst. Growth* 262 (2004) 95.
- [17] I.E. Tyschenko, A.B. Talochkin, A.G. Cherkov, K.S. Zhuravlev, R.A. Yankov, *Solid State Commun.* 129 (2004) 63.
- [18] E.S. Marstein, A. Gunnæs, U. Serincan, S. Jørgensen, A. Olsen, R. Turan, T.G. Finstad, *Nucl. Instr. and Meth. B* 207 (2003) 424.
- [19] E.S. Marstein, A.E. Gunnæs, U. Serincan, R. Turan, A. Olsen, T.G. Finstad, *Surf. Coat. Technol.* 158 (2002) 544.
- [20] F. Iacona, C. Bongiorno, C. Spinella, S. Boninelli, F. Priolo, *J. Appl. Phys.* 95 (2004) 3723.
- [21] J. Heitmann, F. Müller, L. Yi, M. Zacharias, D. Kovalev, F. Eichhorn, *Phys. Rev. B* 69 (2004) 195309.
- [22] J.S. Biteen, N.S. Lewis, H.A. Atwater, A. Polman, *Appl. Phys. Lett.* 84 (2004) 5389.
- [23] U.S. Sias, E.C. Moreira, E. Ribeiro, H. Boudinov, L. Amaral, M. Behar, *Nucl. Instr. and Meth. B* 218 (2004) 405.
- [24] SRIM: The Stopping and Range of Ions in Matter, Program Manual, J.F. Ziegler, 1996.
- [25] U. Serincan, G. Kartopu, A. Guennes, T.G. Finstad, R. Turan, Y. Ekinci, S.C. Bayliss, *Semicond. Sci. Technol.* 19 (2004) 247.
- [26] J.Y. Jeong, S. Im, M.S. Oh, H.B. Kim, K.H. Chae, C.N. Whang, J.H. Song, *J. Lumin.* 80 (1999) 285.
- [27] U. Serincan, G. Aygun, R. Turan, *J. Lumin.* 113 (2005) 229.
- [28] M. Modreanu, M. Gartner, E. Aperathitis, N. Tomozeiu, M. Androulidaki, D. Cristea, P. Hurley, *Physica E* 16 (2003) 461.
- [29] M. Yamamoto, T. Koshikawa, T. Yasue, H. Harima, K. Kajiyama, *Thin Solid Films* 369 (2000) 100.
- [30] R. Turan, T.G. Finstad, *Semicond. Sci. Technol.* 7 (1992) 75.
- [31] S. Margalit, A. Bar-lev, A.B. Kuper, H. Aharoni, A. Neugroschel, *J. Cryst. Growth* 17 (1972) 288.
- [32] Y. Liu, T.P. Chen, Y.Q. Fu, M.S. Tse, J.H. Hsieh, P.F. Ho, Y.C. Liu, *J. Phys. D: Appl. Phys.* 36 (2003) L97.